Proceedings of ASME Turbo Expo 2011
GT2011
June 6-10, 2011, Vancouver, British Columbia, Canada

GT2011-46226

IDENTIFICATION OF SPINNING MODE IN THE UNSTEADY FLOW FIELD OF A LP TURBINE

Davide Lengani, Berardo Paradiso, Andreas Marn, Emil Göttlich
Inst. f. Thermal Turbomachinery and Machine Dynamics
Graz University of Technology, Austria
Email: davide.lengani@tugraz.at

ABSTRACT

This paper presents an experimental investigation of the vane-blade unsteady interaction in an unshrouded LP turbine research rig with uneven blade/vane count (72 blades and 96 vanes). The rig was designed in cooperation with MTU Aero Engines and considerable efforts were put on the adjustment of all relevant model parameters. In particular blade count ratio, airfoil aspect ratio, reduced massflow, reduced speed, Mach and Reynolds numbers were chosen to reproduce the full scale LP turbine at take off condition. Measurements by means of a fast-response pressure probe were performed adopting a phase-locked acquisition technique in order to provide the time resolved flow field downstream of the turbine rotor. The probe has been fully traversed both in circumferential and radial traverses.

The rotor exit is characterized by strong perturbations due to the tip leakage vortex and the rotor blade wake. Circumferential non uniformities due to the upstream vane wake and to the downstream exit guide vane potential effects are also identified. Furthermore in the present configuration with an uneven blade/vane count the non-uniformities due to the stator and rotor row are misaligned along the whole turbine circumference and create a spinning mode that rotates in direction opposite to the rotor at a high frequency. The aeroacoustic theory is employed to explain such further unsteady pattern. The variations of the exit flow angle within a cycle of such pattern are not negligible and almost comparable to the ones within the blade passing period.

NOMENCLATURE

A_m	Circumferential mode amplitude
B_n	Number of blades
BPF	Blade passing frequency
C_{pt}	Total pressure coefficient
g_{vane}	Vane pitch
m	Circumferential mode
M	Mach number
p_t	Total pressure
T	Blade passing period
V_n	Number of vanes
w	relative velocity
α	Flow angle
Ω	Rotor angular velocity
ρ	Flow density

Subscripts

AVE	Circumferentially averaged properties
r	relative

Superscripts

$\bar{}$	Time averaged properties
$\sim$	Ensemble-averaged properties
$\cdot\cdot$	Cycle-averaged properties

INTRODUCTION

The aerodynamic performances of turbine bladings are largely affected by the viscous and potential flow unsteady perturbations. Furthermore the unsteady flow has a strong influence also on blade vibrations and noise emissions. A new generation of low pressure turbines (LPT) is designed in order to fulfill different requirements such as high durability, low noise, high efficiency and low weight. In the last decades, since Binder et al. [1] and Hodson [2], many studies have been performed in turbine research facilities in order to increase the knowledge of the unsteady flow inside a turbine and achieve the different performance parameters.

The sources of unsteadiness are numerous: secondary flows, potential flow fields and wakes are among the main that may be encountered in subsonic turbines. The secondary flows have a considerable effect on the whole flow field of low aspect

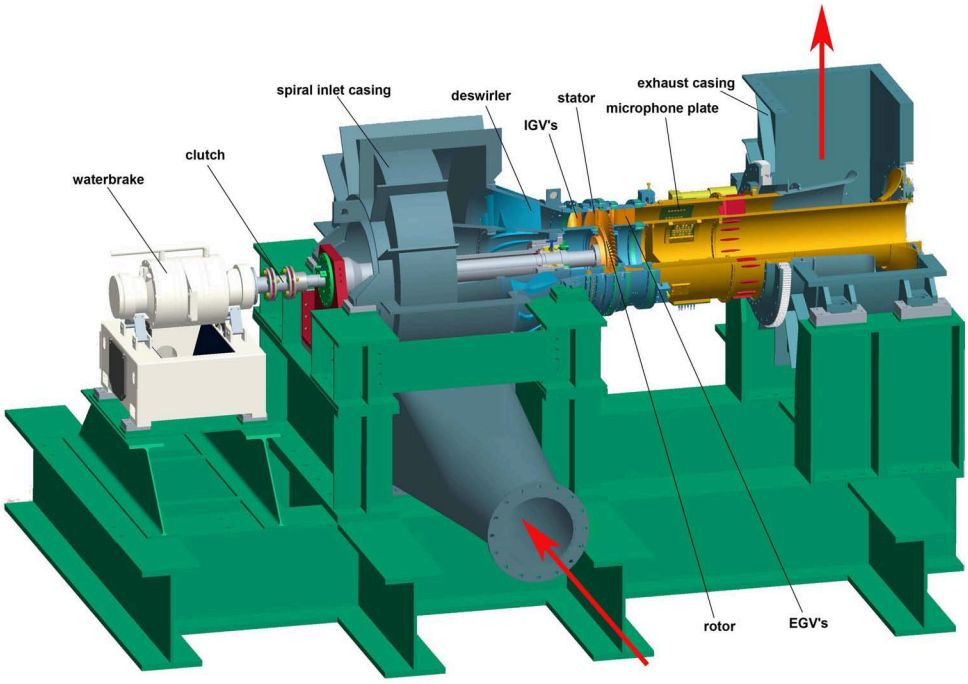

FIGURE 1. SECTIONAL DRAWING OF THE TEST FACILITY, GENERAL ARRANGEMENT.

ratio turbines (e.g. [3–5]) while on high aspect ratio ones, like the case of LPT, their effect is confined in the endwall regions (e.g. [6]). The potential flow interaction of each blade/vane row extends upstream and downstream, as a mutual interaction between adjacent rows, whos relative influence on the flow fields depends on the ratio of stator to rotor pitches [7]. The potential flow field cuts into the wakes propagating from upstream, and the wakes are bowed and stretched as they convect through the rotor blade passages. Furthermore the interaction of the stator wakes with the suction side boundary layer has been the subject of a very large amount of studies since it influences significantly the behaviour of 2D losses (see for example the review by Hodson and Howell [8]).

Stator-rotor interaction represents also a prime mechanism of noise generation, however the blade-vane count ratio may be properly chosen to prevent fundamental tone propagation [9, 10]. The sound propagation of the first harmonic of the blade passing frequency (BPF) may be effectively cut-off in this way (see for example [11]). Such aeroacustic design, involving different vane/blade count, may be properly interfaced with the aerodynamic design. Numerical investigations have shown that the unsteady flow may be inaccurately predicted by blade count modification techniques (e.g. [12, 13]) and fast methods to solve such problem have been proposed (e.g. [14]). However there is a lack of test cases concerning LPT designed for engine-representative conditions that may provide data from both aeroacoustic and unsteady aerodynamic measurements.

The work presented in this paper includes time-resolved area aerodynamic traverses performed on a research low pressure turbine. The test rig is a scaled model of the last 1 and 1/2 stage of a commercial engine and it is operated at engine representative conditions at take-off. A fast response aerodynamic pressure probe (FRAPP) in a three-sensor virtual mode is used to provide the unsteady flow field downstream of the rotor. The paper describes the flow structures in this plane and particular focus is given to the rotating pattern due to the uneven blade/vane count (72 blades and 96 vanes). Such pattern, also called spinning mode, is well known since Tyler and Sofrin [10] and it was shown to be the main reason of tonal noise in the aeroacoustic investigation performed on this test rig by Moser et al. [15].

EXPERIMENTAL FACILITY AND INSTRUMENTATION

Test facility

The Institute for Thermal Turbomachinery and Machine Dynamics (ITTM) at Graz University of Technology operates a 3 MW compressor station to supply a couple of test facilities continuously with pressurized air. In the described test facility, the maximum pressure ratio is 1.6 and the maximum massflow is 15 kg/s. The inflow temperature can be adjusted within a wide range. During tests the mostly used temperature was 100 °C. The pressurized air enters the test facility, shown in Fig. 1, through the spiral inlet casing where the flow turns into axial direction.

In order to provide well defined and uniform inflow conditions, a de-swirler together with a perforated metal plate is mounted downstream of the inlet casing. In the inlet casing, the fixed bearing of the overhung-type turbine shaft is mounted. The shaft power of the test stage drives a water brake, which is connected to the re-cooling plant of the institute. These parts, the inlet casing, the de-swirler, the shaft and the waterbrake are the basic components of the test facility. The de-swirler is followed by the test turbine to be investigated. It consists of the inlet guide vanes (IGV), the stator, the rotor and the exit guide vanes (EGV). The rig is followed by the 360 deg rotatable acoustic measurement section which is equipped with

microphones [15]. Finally, the air leaves the rig through the exhaust casing of the facility into the exhaust stack. A full description of the STTF-test facility is given in Moser et al. [16].

Test turbine

The aerodynamic design of the low pressure turbine was performed by MTU Aero Engines. Considerable effort was put into the adjustment of all relevant model parameters to reproduce the full scale LPT situation. The turbine diameter and the rotating speed are approximately half of those of a commercial aero engine LPT. A section of the rig is shown in Fig. 2 where 0, 1, 2, and 3 indicate the probe measurement positions. The inlet guide vanes (IGV) are pivotable (10 deg) and used to provide some typical pre-swirl in the flow. The IGV is followed by the stator vanes, the rotor and the exit guide vanes (EGV). The 1 and 1/2 stage is representative of the last stage of a commercial engine with turbine exit casing. Table 1 shows the blade count and the main geometrical details of the turbine.

Operating conditions Based on the intended use of the LP turbine rig for acoustic and aerodynamic investigations, the main operating points are selected according to the typical noise certification points, i.e. approach and take-off. The operating points were defined using an aero design point of the last stage of an LP turbine, derived from current LP turbine design practice using scaling along reduced speed, mass flow and pressure ratio. Table 1 shows the reduced mass flow, the reduced speed, and the Reynolds and Mach numbers of the operating point, take-off, at which the aerodynamic investigation discussed in the paper has been carried out. The reduced mass flow and speed are referred to 288.15 K and 1013.25 mbar. The Reynolds and Mach numbers are defined with the midspan conditions at the rotor exit.

Cylindrical high response pressure probe

Unsteady flow measurements were performed by means of a cylindrical single-hole fast-response aerodynamic pressure probe, operated as a virtual three sensor probe for 2D aerodynamic measurements. A miniaturized pressure sensor (Kulite XCE-062) is mounted inside the axis of the probe head, the outer diameter of which is 1.85 mm, more details on the probe design may be found in [17].

The present paper describes the results obtained in an annular sector in plane 2 downstream of the rotor (marked in Fig. 2). The plane is located at 60% of the rotor axial chord downstream of the blade trailing edge. The measurement grid consists of 28 positions along the blade span and of 35 positions over one EGV pitch. The probe aerodynamic accuracy was evaluated in a calibrated nozzle, resulting in an extended uncertainty equal to $\pm 0.5\%$ of the kinetic head for the pressure measurements and equal to ± 0.3 deg for the flow angle. Details on the transfer function of the probe are given in [17] where the probe was calibrated in a low-pressure shock tube. The probe bandwidth is up to 80 kHz, after digital compensation.

Data reduction procedure Data is acquired at 500 kHz for 100 revolutions of the turbine, a total number of

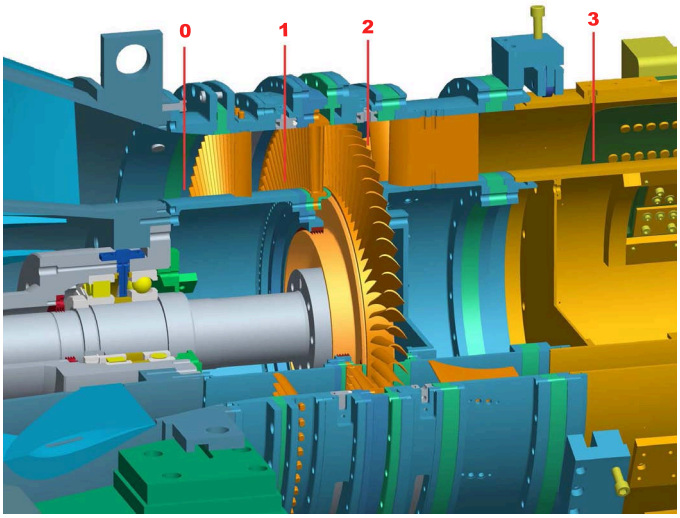

FIGURE 2. SECTIONAL DRAWING OF THE TEST TURBINE, GENERAL ARRANGEMENT; RESULTS DESCRIBED IN THE PAPER REFER TO PLANE 2.

510000 samples are collected in each measuring point. The raw signal is digitally compensated by using the experimental transfer function. Then the "adaptive resampling" process [18] has been applied on the signal: the sampling frequency is adaptively corrected with respect to speed variations of the turbine shaft, by means of the analysis of the shaft encoder signal. In order to respect the probe frequency response the sample rate after resampling is forced to be around 80 kHz. The resampled

TABLE 1. GEOMETRY DETAILS AND FLOW CONDITIONS.

Geometry details	
Number of blades/vanes	
IGV/Stator/Rotor/EGV	83/96/72/15
Stator-rotor axial gap	13 mm
Chord length (Stator at midspan)	19 mm
Chord length (Rotor at midspan)	25 mm
Chord length (EGV)	100 mm
Tip gap	0.8 mm
Tip gap to blade height ratio	1%
Inner diameter	155 mm
Outer diameter	235 mm
Flow parameters	
Reynolds number (rotor exit)	240000
Mach number (rotor exit)	0.53
Reduced massflow	8.97
Reduced rotational speed	5206

data is then phase averaged and at this point the flow properties are derived.

With this procedure there are around 11-12 samples per blade passing period (T), as it may be computed from the sampling frequency after "adaptive resampling" (80 kHz) and the shaft rotational speed. From the spectral analysis of the signal (not shown in the paper) it emerged that almost the whole signal energy is included at the blade-passing frequency and its harmonics. Thus the average among the 72 blade passages has been computed. Due to the high number of blades such average allows the increase of the number of samples in the average-representative blade passing period shown in the paper. The final resolution is equivalent to 40 points, that corresponds to a temporal resolution of $t/T = 0.025$.

The unsteady flow quantities, measured in the absolute frame, are extended to the relative frame to enhance the comprehension of the flow structure of the rotor. The procedure adopted to derive relative quantities is performed accordingly to what described by Gaetani et al. [19].

RESULT AND DISCUSSION

The time-resolved evolution of the flow downstream of the turbine rotor is discussed in this section. Results are presented in Fig. 3 and 4 as contour plots of the relative Mach number in the absolute (stationary) reference frame. These plots are views in the downstream direction on a sector covering one pitch of the exit guide vane and consequently 6.4 pitches of the stator vane and 4.8 rotor blade passages. Figure 3 is the first time-snapshot from Fig. 4 and it is shown in order to underline the basic structures of the flow downstream of the rotor.

The flow features that are caused by the rotor blades, hub

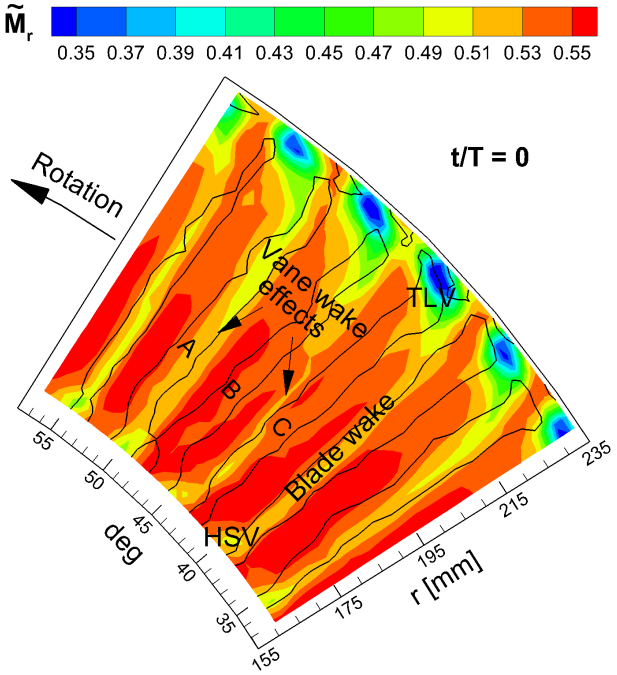

FIGURE 3. TIME-SNAPSHOT OF THE RELATIVE MACH NUMBER; THE DOMINANT STRUCTURES OF THE FLOW ARE MARKED OVER THE EXPERIMENTAL RESULTS.

secondary vortex, the tip leakage vortex and the rotor wake, may be identified in Fig. 3 where their positions are marked over the experimental results. The largest velocity defects occur in the endwall regions. The tip leakage vortex, identified in the picture with the symbol TLV for one blade passage, shows considerably lower relative Mach numbers than the hub secondary vortex (HSV in picture). At the tip there is a very strong interaction between the jet-like leakage flow and the mainstream flow (e.g. [20, 21]) which generates this vortical structure with very low momentum that characterizes around 80% of the blade passage in this region (a similar result was found by [22] for an unshrouded high pressure turbine with moderately high aspect ratio). Furthermore, as observed in many other studies (e.g. [6]) the radial pressure gradient causes fluid to migrate toward the hub. This effect may be observed in the velocity distribution inside the blade passage. The relative Mach number has larger values below midspan than above.

Due to the high aspect ratio of the rotor blade the region between 15% and 80% passage height is characterized by velocity defects related to the blade wakes. In particular the flowfield at the stage exit is the result of two-dimensional interaction mechanisms such as vane wake-blade interaction, which has been largely documented in the last decades since the mid of the 80s [1, 2]. Due to the uneven vane/blade count the shape and the strenght of the wake and consequently of the rotor core flow is not circumferentially constant. Circumferential non-uniformities between adjacent blade passages are marked in Fig. 3 as vane wake effects since they are due to the different interactions between vane wakes and blades. To allow the identification of the stator flow structure positions a iso-contour line of the time-averaged total pressure coefficient is superimposed on the plot of Fig. 3. This total pressure coefficient is defined as the difference between the time-averaged total pressure and its circumferential average and made non dimensional:

$$\overline{C}_{pt} = \frac{\overline{p_t} - p_{t,AVE}}{0.5\rho w_{AVE}^2} \tag{1}$$

Time averaging the total pressure removes the effect of the rotor and thus allows the position of the vane structures position to be determined as performed by [22]. In fact, the number of regions enclosed by the isocountour lines of $\overline{C}_{pt} = -0.02$ corresponds exactly to the number of the upstream stators. It is actually hard to discuss if these regions at negative pressure coefficient, due to the stator structures, are located in the exact correspondence of the stator wakes. As stated by Binder [23] the vane wakes, even if chopped and stretched by the rotor viscous and potential effects, leave the rotor along avenues which are always fixed relative to the upstream vane position. However they interact with the rotor blade boundary layers and according to numerous parameters (blade loading, incidence angle, Reynolds number, inlet turbulence and many others, see for example [8]) they may have positive or negative effects on the boundary layer and loss generation. According to the flow conditions (nominal incidence and high Reynolds number) and turbine geometry, but without numerical or experimental measurements within the blade passage at the present stage, it may be argued that these traces correspond to the stator wake positions.

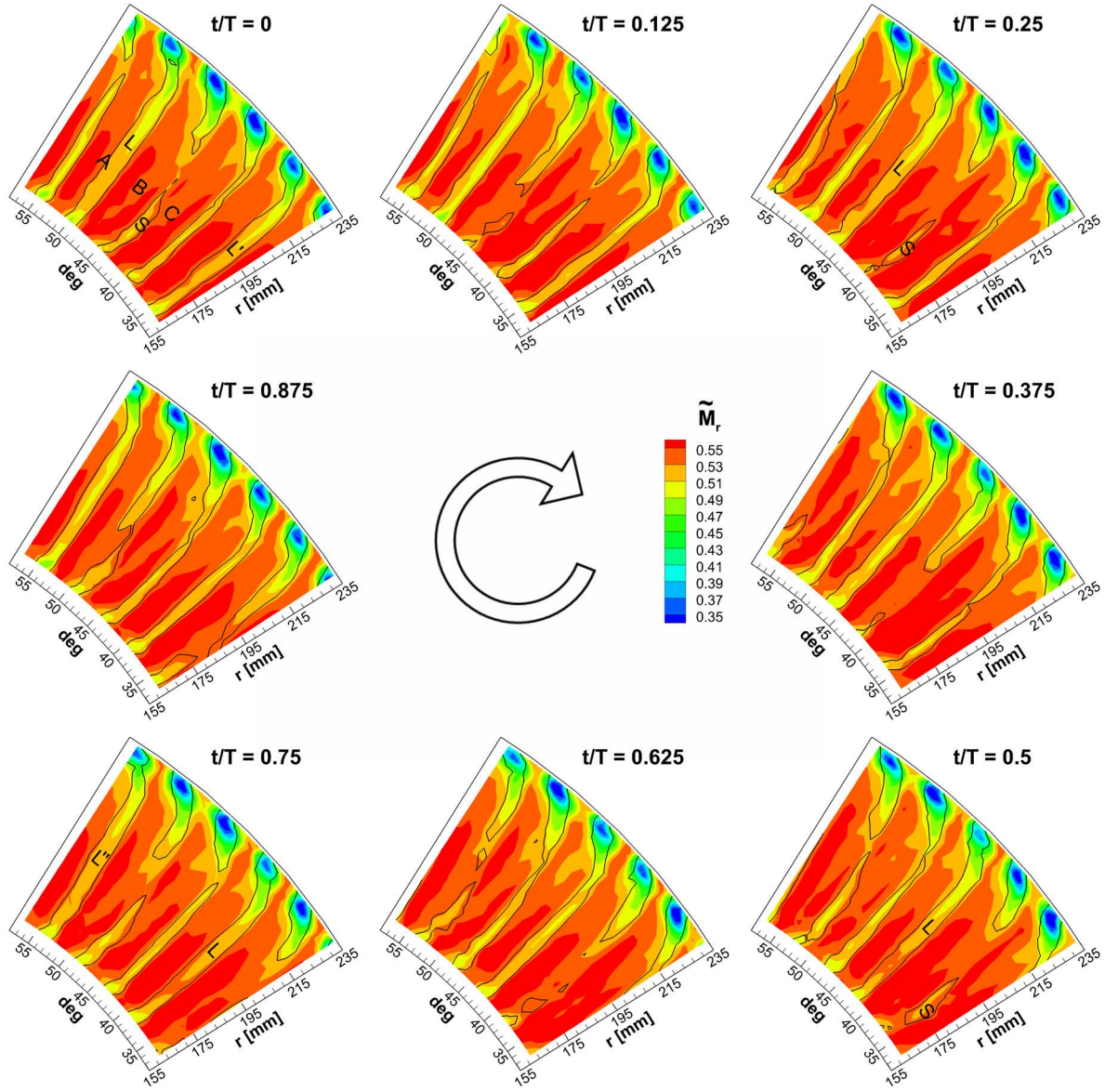

FIGURE 4. TIME-RESOLVED DISTRIBUTION OF THE RELATIVE MACH NUMBER.

The rotor wake is wider in position A (marked in the plot) where it is superimposed on the region at low $\overline{C}_{pt}$. While in positions B and C the areas at low $\overline{C}_{pt}$ are superimposed on the core flow of the rotor and the blade wake between these two positions presents a very low width. A similar distribution may be observed for the hub secondary flows while the opposite trend is shown for the tip leakage vortex, in position A its velocity defect is the lower among the others at different circumferential positions.

Unsteady vane/rotor interaction

The structure of the blade wakes and secondary flows, that depends on their relative position with respect to the vane position, is changing as the rotor moves. The rotor blades on their motion are facing different viscous effects from the stator vanes, these differences may be also associated to a different incidence angle, and consequently a change in the vane/blade mutual potential interactions.

The time-snapshot of Fig. 3 represents just a time instant of the rotor motion in front of the vanes. The complete flow evolution in one blade passing period is depicted in Fig. 4 where eight equidistant time steps are plotted. To help the reader following the evolution of the blade wake structures the iso-contour line of the relative total pressure coefficient is superimposed on each plot. While the vane wake position, fixed in time, may be still identified from Fig. 3. The relative total pressure coefficient is here defined as the difference between the ensemble averaged relative total pressure and its circumferential average and made non dimensional:

$$\tilde{C}_{ptr} = \frac{\tilde{p}_{tr} - p_{tr,AVE}}{0.5\rho w_{AVE}^2} \tag{2}$$

This definition allows the identification of the blade wake and secondary flows within one region, delimited by two iso-contour lines, along the whole span. A value of $\tilde{C}_{ptr} = -5\%$

has been chosen to represent the low momentum areas.

The blade wake with very low width, indicated in Fig. 3 between points B and C, is marked with the letter "S" superimposed on the plot at a circumferential position of around 44 deg in the first time step. A similar flow configuration is visible at the circumferential position of around 40 deg in the time step $t/T = 0.25$ and successively at 35 deg in the time instant $t/T = 0.5$. From this last position it leaves the measurement plane. It is evident that this flow feature rotates clockwise in the area under investigation. This phenomenon may be observed not only for this particular structure but also for the whole flow field. For example also the wake with the largest width identified here with the letter "L", corresponding to point A in Fig. 3, rotates clockwise of around 4 degrees each quarter of the blade passing period. At the same time the tip leakage vortex placed in between the same iso-contour lines shows a local maximum of momentum when compared to the tip leakage vortex of the neighboring blades. The same considerations may be done for the hub secondary vortex positioned within the iso-contour lines of $\tilde{C}_{ptr}$ marked with "S". Furthermore all these flow features are repeated every three blade passages at a fixed time snapshot, see for example the isocountour lines marked as L and L$'$ for $t/T = 0$ and the lines marked as L and L$''$ for t/T =0.75, and they move circumferentially from one time step to the following. Small circumferential variations may be observed within this periodicity of three blade passages and this is due to the potential effects of the downstream vane as it will be shown in the last section of the discussion.

It has to be recalled now that the rotor, in the present view, rotates counterclockwise and that one blade "leaves" the measurement domain during one blade passing period (the eight time snapshots). The rotating pattern here identified instead is rotating clockwise and it moves 15 deg while one blade moves counterclockwise by about 5 deg during the same blade period. It means that the rotating pattern "spins" at a frequency three times larger than the BPF and in the opposite direction.

Modal Theory The knowledge of such rotating pattern, also called spinning mode according to the aeroacoustic theory, is traceable to the early work of Tyler and Sofrin [10]. In particular, according to their theory, for an ideal rotor with identical blades the pressure fluctuations at a circumferential position θ may be written as a Fourier series (e.g. [11]):

$$p(\theta,t) = \sum_{n=-\infty}^{\infty} \sum_{m=-\infty}^{\infty} A_{mn} e^{inB_n\Omega t - im\theta} \tag{3}$$

where n is the harmonic index, Ω the rotor angular velocity, A_{mn} the coefficient of the Fourier series for each harmonic n and for each circumferential mode m. It was shown in [10] that the mode m of the spatial Fourier decomposition is restricted just to some particular values:

$$m = nB_n + kV_n, \;\; with \;\; k = ..., -1, 0, 1, ... \tag{4}$$

Considering just the first harmonic of the blade passing frequency the pressure fluctuation $p(\theta,t)_{n=1}$ can be rewritten as:

$$p(\theta,t)_{n=1} = \sum_{m=-\infty}^{\infty} A_m e^{im(\frac{B_n}{m}\Omega t - \theta)} \tag{5}$$

From this last equation the pressure field may be interpreted as a superposition of an infinite number of rotating patterns, where the number of lobes is given by successive values of m. Each m-lobed pattern rotates at the speed $\frac{B_n}{m}\Omega$ required to generate the first harmonic of the BPF. For the present turbine, where $B_n = 72$ and $V_n = 96$, the possible number of mode m may be expressed:

$$m = 72 + 96k = \; ..., -24, 72, 168, ... \tag{6}$$

The spinning mode previously observed (Fig. 4) corresponds to the mode $m = -24$ of the present theory, which rotational speed is $\frac{B_n}{m}\Omega = -3\Omega$. It should be noted that this theory has been developed for the pressure field while the rotating pattern here identified deals with the aerodynamic flow field. On the other hand Tyler and Sofrin [10] refer to pressure fluctuations as "superposition of effects" which may be thought as viscous and potential effects of each vane or blade row. This is plausible considering that the existence of spinning mode may be observed considering the superposition of any kind of perturbations as discussed in the paper of Tyler and Sofrin [10] (cf. Fig. 16A and 16B of their paper, see Appendix A for more details).

A further extension of the present theory may be done considering that the aeroacoustic theory predicts circumferential and also radial modes inside a turbomachinery duct (e.g. [10, 24]), as it has been experimentally observed by Enghardt et al. [18] and Moser et al. [15]. In the different time steps of Fig. 4 it is possible to identify the break up of the low momentum regions along the radial direction. Break up that appears at different radial positions as this structure rotates. These radial pulsations probably originate from the interaction of the secondary vortices of the stator with the rotor, anyway it seems evident that they may be correlated to radial modes.

Influence of the spinning mode In order to point out the fact that this circumferentially spinning mode represents a further unsteady inflow condition for the following vane row, space-time plots are reported in Fig. 5 and 6. In these plots the circumferential position of the probe normalized with the stator vane pitch y/g_{vane} is plotted on the abscissa, which covers one complete pitch of the exit guide vane, while the normalized time scale t/T is plotted on the ordinate. The real resolution in time of the present measurement ($t/T = 0.025$ instead of the time step 0.25 of Fig. 4) is now adopted. Relative Mach number and relative exit flow angle are displayed in Fig. 5 for midspan and Fig. 6 for three spanwise positions, respectively. It has to be noted that two identical blade passing periods are reproduced on the graph just to make it more clearly readable.

In these diagrams the rotor wakes appear as inclined lines, the inclination of which is the ratio between the number of blades and vanes equal to -0.75, and marked over the experimental data in Fig. 5. The multiple non uniformities at fixed

circumferential positions, with a period y/g_{vane}, are due to the effects of the upstream stator core flow and wakes (as discussed for example in [25]); for clarity three vane wake positions are marked with letters A, B, C as previously identified in Fig. 3. While singular non-uniformities along the whole abscissa are attributable to the potential effects of the downstream exit guide vane. For example for $1 < y/g_{vane} < 3$ the relative Mach number is about 4% lower than for $4 < y/g_{vane} < 6$. The potential effects of the exit guide vane changes according to the blade span (see also Fig. 6) since the EGV is a very low aspect ratio vane and secondary flows becomes predominant in such interaction as described by Miller et al. [26]. Their influence extends upstream and influences the distribution of the relative flow angle and massflow, and as pointed out in the analysis of Fig. 4 it also creates circumferential non-uniformities for the lobed structure of the spinning mode. A similar phenomenon, scattering of the 24-lobe mode due to the number of EGV, has been experimentally observed in the aeroacoustic investigation of Moser et al. [15] performed on this turbine.

The spinning mode appears as an inclined line, the inclination of which is equal to 0.25 and may be derived from the inclination of the rotor structures and the considerations of the previous subsection. This propagation line is marked on Fig. 5. The regions at low momentum of the rotor wakes are positioned along this direction as result of the sum of two causes: rotor-stator interaction and uneven blade/vane count. Structures appear more clearly elongated along the spinning mode direction observing the relative flow angle distribution (Fig. 6). This is particularly evident for midspan and hub positions. At the tip the flow is largely underturned due to the tip leakage vortex and its structures follow again the propagation direction of the rotor-related effects. Nonetheless the flow field is still modulated by the presence of the spinning mode.

Because of this propagation line at a fixed time step (horizontal lines of the diagram), as also observed in Fig. 4, the topology of the velocity defects (wake or secondary flows) is changing considerably within one lobe of the rotating pattern. Furthermore, this unsteady perturbations, due to the 24-lobed spinning mode, rotates at a frequency three times larger than the BPF and represents a pulsed inlet condition for the downstream vane row.

To summarize the effect of the spinning mode on the flow field the average fluctuations of the relative Mach number and exit angle across one period of this phenomenon have been

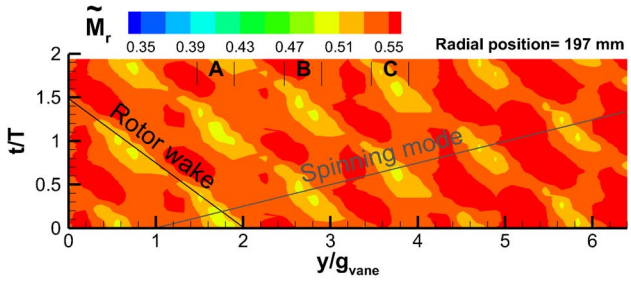

FIGURE 5. SPACE-TIME PLOT OF THE RELATIVE MACH NUMBER. A,B,C CORRESPOND TO THE REGIONS AT $\overline{C}_{pt} \leq -0.02$ MARKED IN FIG. 3.

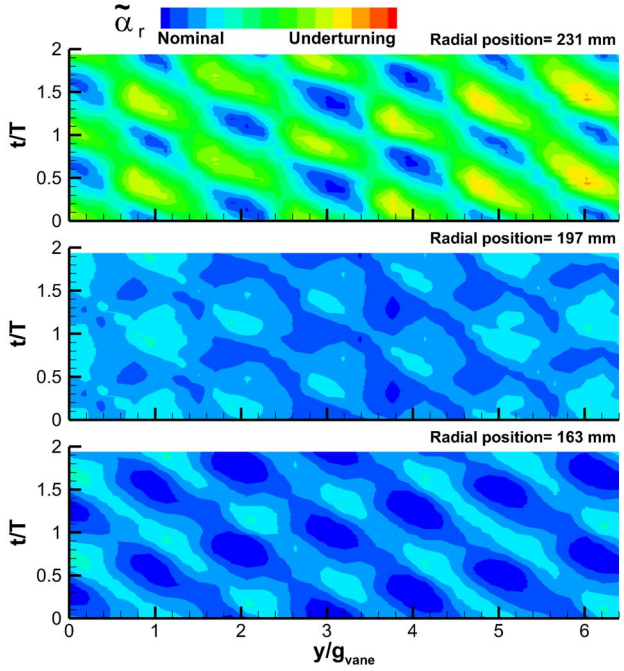

FIGURE 6. SPACE-TIME PLOT OF THE RELATIVE EXIT ANGLE FOR THREE DIFFERENT POSITIONS ALONG THE SPAN.

computed and plotted in Fig. 7 (on top and on bottom, respectively) where they are compared with the fluctuations within the blade passing period.

The average velocity variations across one period of the two periodic patterns are summarized in terms of $\ddot{M}_r/M_{r,AVE}$, where $\ddot{M}_r$ indicates the cycle-averaged value (this procedure is described in details in [27]). The values within each time step of the cycle of the two phenomena are obtained by averaging the phase locked averaged properties on a proper number of circumferential positions. Averages are performed separately in the rotor relative reference system and in the relative system of the spinning mode. The quantity $\ddot{M}_r/M_{r,AVE}$ is very low, around 1%, for the spinning mode both at midspan and at the hub. Whereas the fluctuations due to the rotor passing period are 4% of its mean value at midspan, up to 10% at the hub where the secondary flows have a considerable effect on the velocity distribution. A similar consideration may be done for the tip, not shown here, where fluctuations due to the rotor passing period are 10 times larger than for the spinning mode. The average angle variations are summarized in terms of $\Delta\alpha_r = \ddot{\alpha}_r - \alpha_{r,AVE}$ in Fig. 7 on bottom, where the symbols have the same meaning of the previous definition. Minimum to maximum oscillations of $\Delta\alpha_r$ are up to 2 deg for the spinning mode, and up to 5 deg within the blade passing period. The fact that the angle variations due to the spinning mode are comparable to the variation within the blade passing period while velocity variations are much lower suggests that the generating cause of the spinning mode is correlated mainly to the vane/blade mutual potential interaction. Otherwise if the origin of such phenomenon was found within viscous effects also the velocity variations should have been of comparable intensity.

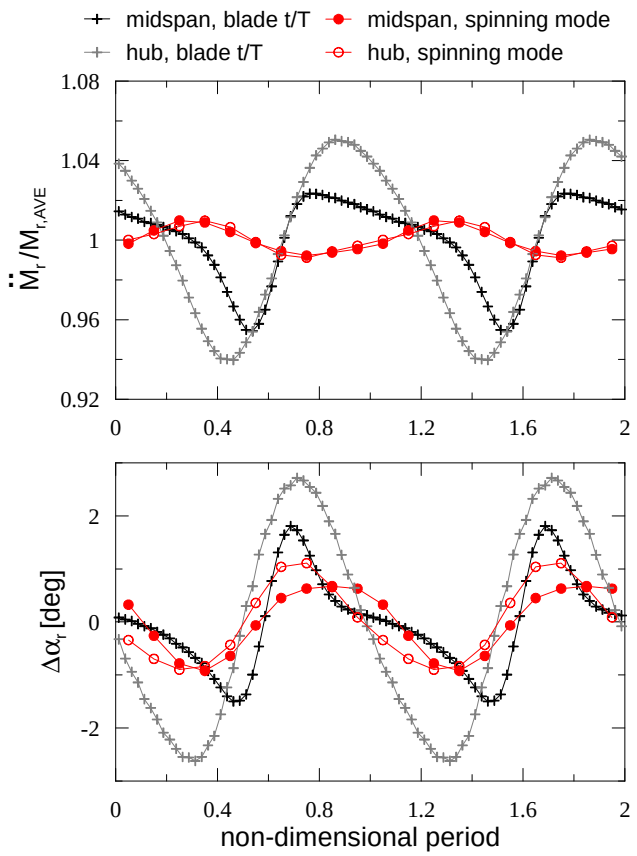

FIGURE 7. AVERAGE VARIATIONS OF THE RELATIVE MACH NUMBER (TOP) AND RELATIVE EXIT ANGLE (BOTTOM) WITHIN TWO CYCLES OF THE TWO PERIODIC PHENOMENA.

Comparison with aeroacoustic results It seems now to be of interest to compare these results with the results of the aeroacoustic investigation of Moser et al. [15]. In summary, in their experimental work the main origin of tonal noise has been found within the 24-lobed mode $m = 72 - 96 = -24$, caused by the stator-rotor interaction. Whereas the higher modes (e.g. m =72, 168), according to the mean flow conditions and turbine rotational speed, have been found to be "cut-off", namely they exponentially decay within the turbine exit duct. On the aerodynamic flow field the traces of structures corresponding to m =72, the signature of the blades, and $m = -24$, the spinning mode due to the uneven blade/vane count, are clearly visible. In particular the viscous flow due the blade wakes do not contribute to the tonal noise propagation since the blade number has been chosen large enough. Furthermore, as previously mentioned, Moser et al. [15] found that the 24-lobed mode was scattered accordingly to the EGV number (15 vanes) in the following modes:

$$m = -24 + 15k = -9, 6, 21 \ \ with \ \ k = 1, 2, 3 \qquad (7)$$

this phenomenon may be justified by the potential flow interaction of the EGV on the rotor flow field as identified in the discussion of Fig. 4 and 6. However such modes were not directly recognized on the aerodynamic flow field since the stator-rotor interaction is more relevant than the rotor-EGV one.

CONCLUSIONS

The development of the unsteady flow downstream of a LP turbine rotor has been reported in the paper. The 1 and 1/2 stage is representative of a modern LP turbine designed for high efficiency and low noise emission operated at engine-representative conditions. Thus the data set provided may be applied for computational code validation. Furthermore, the time resolved measurements have been used to discuss in details the features that characterize the unsteady flow field.

The tip-leakage vortex, hub secondary flow, rotor wake and potential effects from the downstream EGV have been identified on the rotor outlet flow. All these features are influenced by the viscous and potential interactions of the upstream stator. Hence, as the rotor moves each blade passage experiences variations in the wake and secondary flow extension. Furthermore, in the present configuration, designed with an uneven blade/vane count in order to reduce the tonal noise propagation, the superposition of perturbations from the stator and rotor blade row generates a rotating pattern. The characteristics of the spinning mode, lobed structure and spinning rotational speed directly depend, according to the aeroacoustic theory, on the blade to vane count ratio. The fluctuations of the flow quantities within a cycle of this periodic pattern are related to the stator/rotor mutual potential interaction and may influence the aerodynamic behaviour of the downstream rows. In particular, in the stationary frame of reference the flow may be considered as the superposition of rotating patterns: the flow features of the rotor blade and the flow configuration due to the spinning mode.

ACKNOWLEDGMENT

Paolo Gaetani and Giacomo Persico from Politecnico di Milano are gratefully acknowledged for their support and manufacturing and calibration of the FRAPP. The authors would like to thank H.P. Pirker for operating the compressor station. Thanks to M. Moser for his support. Further the EU project VITAL, contract no. AIP4-CT-2004-012271, is acknowledged in which the stage was designed, manufactured and operated.

REFERENCES

[1] Binder, A., Förster, W., Kruse, H., and Rogge, H., 1985. "Experimental investigation into the effect of wakes on the unsteady turbine rotor flow". *ASME Journal of Engineering for Gas Turbines and Power,* ***107***(2), pp. 458–465.

[2] Hodson, H. P., 1985. "Measurements of wake-generated unsteadiness in the rotor passages of axial flow turbines". *ASME Journal of Engineering for Gas Turbines and Power,* ***107***(2), pp. 467–476.

[3] Sharma, O. P., Pickett, G. F., and Ni, R. H., 1992. "Assessment of unsteady flows in turbines". *ASME Journal of Turbomachinery,* ***114***, January, pp. 79–90.

[4] Pullan, G., 2006. "Secondary flows and loss caused by

blade row interaction in a turbine stage". *ASME Journal of Turbomachinery,* ***128***, July, pp. 484–491.

[5] Persico, G., Mora, A., Gaetani, P., and Savini, M., 2010. "Unsteady aerodynamics of a low aspect ratio turbine stage: Modeling issues and flow physics". In Proceedings of ASME Turbo Expo 2010, June 14–18, Glasgow, UK, ASME Paper No. GT2010-22927.

[6] Arndt, N., 1993. "Blade row interaction in a multistage low-pressure turbine". *ASME Journal of Turbomachinery,* ***115***, January, pp. 137–146.

[7] Korakianitis, T., 1992. "Blade-loading effects on the propagation of unsteady flow and on forcing functions in axial-turbine cascades". *Journal de Physique III,* ***2***(2), April, pp. 507–525.

[8] Hodson, H. P., and Howell, R. J., 2005. "The role of transition in high lift low pressure turbines for aero engines". *Progress in Aerospace Science,* ***41***(6), August, pp. 419–454.

[9] Groeneweg, J. F., Sofrin, T. G., Rice, E. J., and Gliebe, P. R., 1991. "Turbomachinery noise". In *Aeroacoustics of Flight Vehicles: Theory and Practice, Vol. 1: Noise Sources*, H. Hubbard, ed., NASA RP-1258. ch. 3, pp. 151–209.

[10] Tyler, J. M., and Sofrin, T. G., 1962. "Axial flow compressor noise". *SAE Transaction,* ***70***, pp. 309–332.

[11] Rienstra, S. W., and Hirschberg, A., 2004. *An Introduction to Acoustics*. Eindhoven University of Technology.

[12] Arnone, A., and Pacciani, R., 1996. "Rotor-stator interaction analysis using the navier-stokes equation and a multigrid method". *ASME Journal of Turbomachinery,* ***118***, October, pp. 679–689.

[13] Dorney, D. J., Flitan, H. C., Ashpis, D. E., and Solomon, W. J., 2000. "The effects of blade count on boundary layer development in a low-pressure turbine". In 38th Aerospace Sciences Meeting and Exhibit, Reno, Nevada, January 10-13, Paper No. AIAA-2000-0742.

[14] Gerolymos, G. A., Michon, G. J., and Neubauer, J., 2002. "Analysis and application of chorochronic periodicity in turbomachinery rotor/stator interaction computations". *Journal of Propulsion and Power,* ***18***(6), November, pp. 1139–1152.

[15] Moser, M., Tapken, U., Enghardt, L., and Neuhaus, L., 2009. "An investigation of low pressure turbine blade-vane interaction noise: Measurements in a 1.5-stage rig". *Proceedings of the Institution of Mechanical Engineers, Part A: Journal of Power and Energy,* ***223***(6), pp. 687–695.

[16] Moser, M., Kahl, G., Kulhanek, G., and Heitmeir, F., 2007. "Construction of a subsonic test turbine facility for experimental investigations of sound generation and propagation for low pressure turbines". In ISABE conference Beijing, Paper No. ISABE-2007-1366.

[17] Persico, G., Gaetani, P., and Guardone, A., 2005. "Design and analysis of new concept fast-response pressure probes". *Meas. Sci. Technol.,* ***16***, pp. 1741–1750.

[18] Enghardt, L., Tapken, U., Neise, W., Kennepohl, F., and Heinig, K., 2001. "Turbine blade/vane interaction noise: Acoustic mode analysis using in-duct sensor rakes". In Proceedings of the Seventh AIAA/CEAS-Aeroacoustics Conference, Maastricht, The Netherlands, 28-30 May, Paper No. 2001-2153.

[19] Gaetani, P., Persico, G., Dossena, V., and Osnaghi, C., 2007. "Investigation of the flow field in a high-pressure turbine stage for two stator-rotor axial gaps-part 2: Unsteady flow field". *ASME Journal of Turbomachinery,* ***129***, July, pp. 580–590.

[20] Bindon, J. P., 1989. "The measurement and formation of tip leakage loss". *ASME Journal of Turbomachinery,* ***111***, July, pp. 257–263.

[21] Arts, T., 2004. *Turbine Blade Tip Design and Tip Clearance Treatment*. VKI Lecture Series, LS 2004-02.

[22] Miller, R. J., Moss, R. W., Ainsworth, R. W., and Harvey, N. W., 2003. "The development of turbine exit flow in a swan-necked inter-stage diffuser". In Proceedings of ASME Turbo Expo 2003, June 16-19, Atlanta, Georgia, USA, ASME Paper No. GT-2003-38174.

[23] Binder, A., Schröder, T., and Hourmouziadis, J., 1989. "Turbulence measurements in a multistage low-pressure turbine". *ASME Journal of Turbomachinery,* ***111***(2), April, pp. 153–161.

[24] Eversman, W., 1991. "Theoretical models for duct acoustic propagation and radiation". In *Aeroacoustics of Flight Vehicles: Theory and Practice, Vol. 2: Noise Control*, H. Hubbard, ed., NASA RP-1258. ch. 13, pp. 101–163.

[25] Canepa, E., Formosa, P., Lengani, D., Simoni, D., Ubaldi, M., and Zunino, P., 2007. "Influence of aerodynamic loading on rotor-stator aerodynamic interaction in a two-stage low pressure research turbine". *ASME Journal of Turbomachinery,* ***129***, October, pp. 725–732.

[26] Miller, R. J., Moss, R. W., Ainsworth, R. W., and Harvey, N. W., 2004. "The effect of an upstream turbine on a low-aspect ratio vane". In Proceedings of ASME Turbo Expo 2004, June 14-17, Vienna, Austria, ASME Paper No. GT-2004-54017.

[27] Zaccaria, M. A., and Lakshminarayana, B., 1997. "Unsteady flow field due to nozzle wake interaction with the rotor in an axial flow turbine: Part 1 – rotor passage flow field". *ASME Journal of Turbomachinery,* ***119***, April, pp. 201–213.

APPENDIX A: DEMONSTRATION OF ROTATING PATTERNS

As stated in the paper of Tyler and Sofrin [10] the existence of spinning modes may be shown by means of a simple demonstration involving reasonably few blades and vanes. Figure 8 illustrates in diagram the case of a 6-blade rotor interacting with an 8-vane stator, where the ratio of vane to blade has been kept constant with the stage presented in the paper. Equation 5 predicts the existence of a pattern turning at $-6/2 = -3$ times the shaft speed, where the minus indicates counter rotation. The rotor blades (red colour) are represented by six spokes, one of which is marked with a large dot for identification of rotor position. The eight stator vanes are shown in black colour as short radial segments extending inward from the duct wall. In the first diagram, the marked blade coincides with the upper stator, the coincidence is identified with a large blue dot. Successive pictures show intermediate positions of the rotor (red dot) and the coincidence (blue dot) as the rotor makes 1/8 of a turn. Notice that in this time interval, the coincidence position has been moved of 3/8 of a turn in the opposite direction, and is therefore turning at a rate of 3 times the rotor speed in the opposite direction.

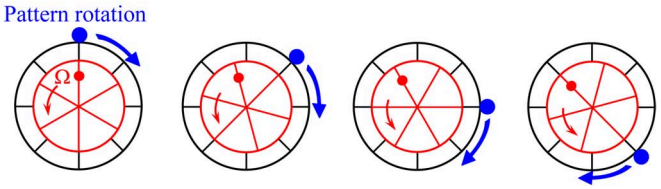

FIGURE 8. DEMONSTRATION OF ROTOR-STATOR INTERACTION PATTERNS, ADAPTED FROM [10]